RSC Advances

ROYAL SOCIETY OF CHEMISTRY

www.rsc.org/advances

Smart Magnetic Nanosystem with Controllable Drug Release and Hyperthermia for Potential Cancer Therapy

Yi Xu[a], Yufang Zhu[b*], Stefan Kaskel[c]

[a] School of Medical Instrument and Food Engineering, University of Shanghai for Science and Technology, 516 Jungong Road, Shanghai 200093, China

[b] School of Materials Science and Engineering, University of Shanghai for Science and Technology, 516 Jungong Road, Shanghai 200093, China

[c] Professur f¨ur Anorganische Chemie I, Fachrichtung Chemie und Lebensmittelchemie, Technische Universit¨at Dresden, Bergstrasse 66, Dresden, 01062, Germany

*Corresponding authors: Prof. Yufang Zhu

Tel: +86-21-55271663;

Email: zjf2412@163.com

Abstract: We have successfully constructed a smart therapeutic platform with potential controllable drug release and magnetic hyperthermia through the conjugation of carboxyl-modified DNA_{20} onto the aminated magnetic mesoporous silica nanoparticles (MMSNs). Drug release behavior, magnetic heating capacity, in vitro cytotoxicity, and cell uptake of the magnetic nanosystem were evaluated. The results showed that magnetic nanosystem could control the doxorubicin (DOX) release behavior with reversible temperature response. Also, the MMSN-NH_2 nanoparticles could efficiently generate heat upon exposure to an alternating magnetic field due to their superparamagnetic behavior. Furthermore, the MMSN-NH_2 nanoparticles could be effectively taken up by HeLa cells, and negligible cytotoxicity has been observed for the MMSN-NH_2 nanoparticles. Therefore, magnetic nanosystem had potential for cancer therapy with controlled drug release and magnetic hyperthermia.

1. Introduction

Combination of nanotechnology with chemotherapy and hyperthermia can avoid several critical clinical problems of free anticancer drugs: low solubility, serious toxicity, unfavorable pharmacokinetics and poor biocompatibility [1,2]. Engineering of nanosystem with stimuli-responsive performances has been considered as a highly desirable strategy for the successful cancer treatment [3,4]. Studies demonstrated that magnetic mesoporous silica nanoparticles (MMSNs) based therapeutic platform can realize the on-demand drug release triggered by temperature change [5-7]. On the other hand, magnetic nanoparticles can generate heat under an alternating magnetic field due to the Néel and Brownian relaxation or hysteresis loss, which has been applied for magnetic hyperthermia therapy. Under the help of nanotechnology, chemotherapy together with hyperthermia could significantly improve the therapy efficiency [8-10].

Recently, much effort has been made to develop smart therapeutic platform which can specifically target the disease site and control the drug release behavior, e.g. “zero release” before arriving at target cells or tissues is necessary. The selection of appropriate ingredients, which can be activated by stimuli to control the drug release and stable enough under physiological conditions, is attractive [11]. Light [12,13], pH change [12,14], enzymatic activity [15,16], redox activation [17], and temperature change [18] are widely used to trigger the drug release. Among them, temperature-triggered drug release is relatively more preferable because the local body temperature can change with ambient conditions [19]. A variety of chemical

ingredients which own temperature-responsive property have been introduced to regulate the release of cargo loaded in the carriers [20-22]. Liu et al. reported that by the introduction of 1-tetradecanol (melting temperature about 39°C) into drug delivery system, the “zero premature release” could be realized under the help of the phase-change molecules [20]. N-isopropylacrylamide is another kind of temperature responsive polymer, and widely used in drug delivery system [22-25]. However, these responsive polymer-based controllers showed either complicated coating process of temperature-responsive materials or not suitable phase-change temperature in the range of body temperature.

DNA is biocompatible and easy to synthesize. Many studies showed that compare with temperature-responsive polymers, DNA-capped drug delivery system is more suitable and smart to control drug release behavior upon exposure to a specific stimulus [26-29], and it provides a new possibility for clinical application. Many DNA-capped drug delivery systems have been reported [30-32]. The advantage of using DNA as gatekeeper lies on the changeable chain length, variations in G/C content in DNA chains and even the size and surface density of oligonucleotides attached to the nanoparticles can lead to tunable temperature response feature [33-34]. Derfus et al. report a remotely-actuated delivery system, DNA with different chain length self-assembles on the superparamagnetic nanoparticles, the radiofrequency electromagnetic field (EMF) can stimuli the heat-labile linker through different temperature [34]. Yu et al. studied the relationship between chain length of DNA and the critical stimuli temperature. MSNs-based drug delivery system was

capped with different length of single-stranded DNA, and the gate opened and the cargo released when the temperature increase. Furthermore, the stimuli temperature increased as the length of DNA became longer [35]. Ruiz-Hernandez et al. develop another kind of “on-off” release system through the hybridization of double DNA strands as gatekeeper [31]. Therefore, DNA-capped nanosystem could be a promising therapeutic platform for potential cancer therapy.

Furthermore, magnetic nanoparticles could arrive at the disease sites efficiently under the guidance of external magnetic field, and could control the drug release manner through the temperature increase generated by the alternating magnetic field. Thus, DNA-capped mangetic nanosystem could effectively mitigate the side-effects caused by toxic drugs to normal tissues [36,37], and the therapeutic efficiency against cancer cells could be significantly enhanced. Recently, our group developed DNA-capped magnetic nanoparticles for potential controlled drug release, and the result indicated that DNA could successfully cap the drug inside the mesopores [38]. However, the capping process was complicated and not easy to control, and the force between the hybridization of DNA strands was too strong, which hinder the drug release efficiency.

In this study, we constructed a DOX/MMSN-NH_2/DNA_{20} based smart therapeutic platform by the conjugation of carboxyl-modified DNA onto the aminated MMSNs (scheme 1). Fe_3O_4 nanoparticles serve as magnetic core inside the nanosystem with mesoporous silica coatings and DNA serve as gatekeeper to cap the mesoporous outlets. The capping process was simple, reliable and well controllable. On the other

hand, The carboxyl-modified DNA_{20} was anchored to the amino group on the surface of DOX/MMSN-NH_2, the formed amide bond was stable enough even when the temperature increases to 43°C, while the electrostatic interaction between negative charged DNA_{20} and positive charged DOX/MMSN-NH_2 was relative weak and easily be destroy when the temperature increased above 43 ^{o}C [13,26,35]. Thus, the appropriate force between DNA and the surface of MMSNs induced the reversible temperature responsive conjugation. Therefore, the smart nanosystem showed synergistic functions: the mesoporous channels can provide efficient space for drug loading, and the "gatekeeper" DNA can control the drug release behavior with reversible manner. At the same time, a magnetic hyperthermia performance can be realized due to the magnetic core through the alternating magnetic field, and the temperature increase can trigger the drug release.

2. Experimental Section

2.1. Chemicals and Materials

Tetraethylorthosilicate (TEOS), triethanolamine (TEA), toluene, ethanol, hydrochloric acid (HCl, 37%) , potassium dihydrogen phosphate (KH_2PO_4), sodium hydroxide (NaOH), ferric chloride ($FeCl_3.6H_2O$), ferrous chloride ($FeCl_2.4H_2O$), 1-ethyl-3-(3-dimethylaminopropyl) carbodiimide (EDC), N-Hydroxysuccinimide (NHS), 2-(N-Morpholino) ethanesulfonic acid monohydrate (MES), were obtained from Sinopharm Chemical Reagent Co. Ltd., doxorubicin hydrochloride (DOX), was obtained from Sangon Biotech (Shanghai) Co. Ltd., Hexadecyltrimethylammonium

p-toluenesulfonate (CTAT) and 3-aminopropyltriethoxysilane (APTES) were obtained from Sigma-Aldrich. Ultrapure water was obtained from Millipore pure water system. All chemicals were of analytical-reagent grade and used without further purification. Oligonucleotides were purchased from Sangon Biotech (Shanghai) Co. Ltd., the sequences of DNA_{20} are 5'-COOH-$(CH_2)_6$-ACT CCT GGT ATG TAG CGC TA.

2.2. Synthesis and modification of MMSNs

MMSNs were synthesized according to the previously reported method [39]. Amino groups were grafted onto MMSNs to form MMSN–NH_2 nanoparticles as follows: 500 mg of the calcined MMSNs were suspended in 40 ml of anhydrous toluene by ultrasonication, afterward the mixture was heated to 100 °C to remove water, subsequently, 0.75ml APTES was added into the mixture and the mixture was refluxed for 20 h under nitrogen atmosphere. The resulting products were collected by centrifugation and washed with toluene for several times to eliminate un-reacted moieties. Finally the as-modified nanoparticles were dried under vacuum at 60°C for 24 h.

2.3. Characterization

Scanning electron microscopy (SEM) was carried out using an FEI Quanta 450 field emission scanning electron microscope. Transmission electron microscopy (TEM) images were obtained on a JEM-2100F transmission electron microscope. N_2 adsorption–desorption isotherms were obtained on a Micromeritics Tristar 3020

automated surface area and pore size analyzer at -196 ^{o}C under continuous adsorption conditions. Brunauer–Emmett–Teller (BET) and Barrett–Joyner–Halenda (BJH) methods were used to determine the surface area and mesopore size distribution. Dynamic light scattering (DLS) and zeta potential measurements were performed on a Malvern zeta-sizer Nano-ZS90. Fourier transform infrared (FTIR) spectra were recorded on a LAM750(s) spectrometer in transmission mode. UV–vis absorption spectra were measured on a NanoDrop 2000C spectrophotometer. Thermo-gravimetric (TG) analysis was performed on a DMA-8000 dynamic mechanical thermal analyzer. Magnetic heating curves of MMSN nanoparticles were obtained on a DM100 magnetic hyperthermia analyzer (NanoScale Biomagnetics, Spain) at a magnetic field of 180 Gauss and a frequency of 409 kHz. Magnetization curve was carried out using a TFWI-ZDYP V 3.0.4 vibrating sample magnetometer (VSM) at 298 K.

2.4. Preparation of DOX/MMSN-NH_2/DNA_{20} complexes

DOX/MMSN-NH_2/DNA_{20} complexes were prepared according to a previously reported method with some modifications [35]. Briefly, 5 mg MMSN-NH_2 was added and dispersed in 10 ml DOX solution (0.5 mg/ml), the mixture was stirred under dark conditions at the room temperature for 24 h. The solution was centrifuged (12000 rpm, 10 min) and washed with water for three times to remove the DOX molecules adsorbed physically on the outer surface of the MMSN-NH_2 nanoparticles. The precipitates were redispersed in 5 ml MES buffer (10 mM, pH=6.0) for further use.

Carboxyl-modified DNA with 20 bases (DNA_{20}) were diluted in ultrapure water to a concentration of 100 μM and stored at −20 °C until use.

DOX/MMSN-NH_2/DNA_{20} complexes were obtained by coupling the carboxyl group of the oligonucleotide and the amino group on the surface of MMSN-NH_2 nanoparticles to form the amide bond. Firstly, 8.9 μl EDC solution (2.8mM) was added to 50 μl DNA_{20} (100 μM) solution, the mixture was reacted for 10 min, and then 2 μl NHS solution (2.8 mM) was added, another 20 min reaction was needed to activate carboxylate groups. Then, the mixture was added to 2 ml DOX/MMSN-NH_2 solution with gentle shaking in darkness. The solution was reacted for 24 h for the formation of the amide bond. Because the single stranded DNA_{20} was negatively charged, it could be adsorbed on the surface of MMSN-NH_2 nanoparticles through electrostatic interaction, and the mesoporous outlets in the MMSN-NH_2 nanoparticles could be capped by DNA_{20} and DOX molecules could be prevented from leaking. After that, the precipitates were centrifuged (12000 rpm, 10 min) and washed with PBS buffer for three times and finally redispersed in 2 ml PBS buffer.

2.5. DOX release from DOX/MMSN-NH_2/DNA_{20} complexes

In vitro release of DOX from the DOX/MMSN-NH_2/DNA_{20} complexes were carried out in PBS buffer with different temperature. The obtained DOX/MMSN-NH_2/DNA_{20} complexes were dispersed into 2 ml PBS buffer at 37°C, 43°C and 47°C respectively. After a predetermined time interval, 6 μl of the suspension was collected and centrifuged, and the supernatant was used for quantitative analysis of the released DOX with NanoDrop 2000C spectrometer. The controllable

release behavior of DOX/MMSN-NH_2/DNA_{20} complexes was further analyzed with a high-low temperature cycle. Briefly, 2 ml DOX/MMSN-NH_2/DNA_{20} complexes in PBS buffer was heated in water bath for six high-low cycles (37°C-43°C), for each cycle, the complexes was first heated at 43°C for one hour and then the complexes was cooled down to room temperature, the released DOX was measured by the same method as mentioned above. Next, the complexes were kept at 37°C for 12 h, and measured the released DOX again. Before determination, a calibration curve was recorded by measuring the absorbance values at the absorbance of DOX at 488 nm.

2.6. Magnetic heating capacity of MMSN-NH_2 nanoparticles

The magnetic heating capacity of MMSN–NH_2 nanoparticles were evaluated using a DM100 System (NanoScale Biomagnetics, Spain) and the temperature was measured with an optical fiber temperature sensor. MMSN–NH_2 nanoparticles were dispersed in water with a concentration of 10, 20, 30, 40 or 50 mg/ml. The suspension was heated under an alternating magnetic field with the strength of 180 Gauss and the frequency of 409 kHz for 10 min.

2.7. Cell culture

HeLa cells were grown in MEM medium, supplemented with 10% FBS, 100 U/ml penicillin, 100 mg/ml streptomycin at 37 °C in humidified air containing 5% CO_2. HeLa cells were cultured according to the manufacturer's instructions.

2.8. In vitro cytotoxicity assay

An in vitro cytotoxicity assay for the MMSN–NH_2, DOX/MMSN-NH_2,and DOX/MMSN-NH_2/DNA_{20} complexs were performed using a Cell Counting Kit-8 (CCK-8, Dojindo, Japan). HeLa cells were seeded into a 96-well plate at a density of 5000 cells per well. After seeding the cells, the MMSN–NH_2, DOX/MMSN-NH_2, and DOX/MMSN-NH_2/DNA_{20} complexes solutions (1 mg/ml in MEM medium) were immediately added into a 96-well plate. The final concentrations of the MMSN–NH_2, DOX/MMSN-NH_2, and DOX/MMSN-NH_2/DNA_{20} complexes were 0, 25, 50, 75 and 100 μg/ml, and the final medium volume in each well was 100 μl. After incubation of cells for 24h, 10 μl of CCK-8 solution was added into each well, and the cells were incubated for another 3 h. The absorbance at 450 nm was then measured using a microplate reader (MTP-880 Lab, Corona, Japan). Cytotoxicity was expressed as the percentage of viable cells compared with that of untreated control cells.

To investigate if the therapeutic effect of hyperthermia and chemotherapy could be controlled by using the magnetic nanosystems, two high-low temperature cycles were performed to the nanosystems for cell culture. After seeding the HeLa cells, the MMSN–NH_2, DOX/MMSN-NH_2, and DOX/MMSN-NH_2/DNA_{20} complexes solutions (1 mg/ml in MEM medium) were immediately added into a 96-well plate with a final concentration of 100 μg/ml. After incubation of cells for 24h, the cells were cultured at 43°C for 30 min, and then moved to 37 °C for 24h culture. Finally, CCK-8 solution was added to investigate the cell viability. Another group was treated for two high-low cycles for further study.

2.9. Cell uptake assay

For the investigation on cell uptake of DOX/MMSN-NH_2 nanoparticles, DOX/MMSN-NH_2 nanoparticles and Fluorescein isothiocyanate (FITC)-labeled DOX/MMSN-NH_2 nanoparticles (DOX/MMSN-NH_2-FITC) were used to investigate cell uptake efficiency. In a typical procedure, HeLa cells were seeded in a 35 mm glass bottom Petri dish at a density of 1.0×10^5 cells. After incubation of cells for 24 h, DOX/MMSN-NH_2 nanoparticles and DOX/MMSN-NH_2-FITC nanoparticles were added in the dish at a final concentration of 100 μg/ml. When the cells had been incubated for another 6 h, the culture medium was removed, and the cells were washed with PBS twice. Subsequently, the cells were fixed with 4% paraformaldehyde for 15 min and stained with DAPI (1μg/ml) for 15 min using a standard procedure. Finally, all of the samples were visualized using a confocal laser scanning microscope (CLSM, SP5, Leica).

3. Results and discussion

3.1 Characterization of MMSN–NH_2 nanoparticles

Amino-functionalized MMSNs (MMSN-NH_2) were synthesized by grafting amino groups onto the surface of MMSNs through the post grafting method using 3-aminopropyltriethoxysilane. The representative SEM and TEM images of as-prepared MMSN-NH_2 nanoparticles are shown in Fig.1. The monodisperse and spherical nanoparticles indicated that amino modification did not induce aggregates

of MMSNs. The narrow particle size distribution from the dynamic light scattering (DLS) analysis also confirmed the good dispersity of MMSN-NH_2 nanoparticles. As shown in TEM image, the magnetic core (Fe_3O_4) and dendritic mesoporous channels could be clearly observed in each MMSN-NH_2 nanoparticles. The structure characteristics facilitate drug loading and delivery. N_2 adsorption–desorption measurement in Fig. 2 shows a typical type IV isotherm, indicative of a mesoporous structure, which were consistent with the TEM result. The Brunauer-Emmett-Teller (BET) surface area of MMSN-NH_2 nanoparticles was 172 m^2/g and the pore volume was about 0.4 cm^3/g (Fig.2). Compared with MMSNs (500 m^2/g of BET surface area and 0.79 cm^3/g of pore volume), the decrease of BET surface area of MMSN-NH_2 nanoparticles could be due to the large amount of amino groups were introduced onto the surface of MMSNs. TG analysis (Fig.3) showed that the weight loss from room temperature to 225 ^oC was the adsorbed H_2O in the MMSN-NH_2 nanoparticles, and about 11.5% of weight loss from 225 ^oC to 800 ^oC was attributed to the amino groups grafted on the surface of MMSNs. Zeta potentials were measured when all samples were dissolved in water with a concentration of 1 μg/μl. As shown in Fig. 4, zeta potential value of the magnetic nanoparticles was reversed from -13.7 mV to 16.4 mV due to the successful grafting of positively charged amino groups onto the surface of MMSNs. FTIR spectra analysis further verified the grafting of amino groups onto the surface of MMSNs. As shown in Fig. 5, after MMSNs were modified with amino groups, the appearance peak at 1496 cm^{-1} can be attributed to the bending vibration of N–H groups. At the same time, the Si–OH band at 960 cm^{-1} in the

MMSNs spectrum became significantly weaker after modifying with amino groups.

3.2. Preparation of the DOX/MMSN–NH_2/DNA_{20} complexes and the temperature–responsive anticancer drug release

Anticancer drug, doxorubicin (DOX), was used as a model drug owing to its good anticancer activity against several kinds of tumors [38]. DOX was introduced into the MMSN-NH_2 nanoparticles, and then the carboxyl modified DNA_{20} was used to cap the mesoporous outlets through the amidation reaction. As shown in Fig. 6, the appearance of the peak at 488 nm for DOX/MMSN-NH_2 was attributed to the DOX absorbance, indicating the successful loading of DOX into the MMSN-NH_2 nanoparticles. On the other hand, the decrease of BET surface area from 172 m^2/g to 130 m^2/g (data not shown) also suggested the successful loading of DOX into the MMSN-NH_2 nanoparticles. UV-vis analysis was applied to quantify the DOX loading capacity in the MMSN-NH_2 nanoparticles. The loaded amount of DOX in the MMSN-NH_2 nanoparticles was estimated to be ca. 64 μg /mg, which was determined from the difference in the DOX concentration between the initial solution and the residual supernatant according to the calibration curve prepared before. TG analysis was further used to confirm the loading capacity of DOX in the MMSN-NH_2 nanoparticles. The DOX/MMSN-NH_2 complexes showed 16.5% of weight loss from 225 ^oC to 800 ^oC. Compared to the 11.5% of weight loss from the MMSN-NH_2 nanoparticles, the DOX loading capacity could be estimated to be 5% in the MMSN-NH_2 nanoparticles, which is consistent with the UV-vis analysis.

Carboxyl-modified DNA_{20} was used to cap the mesoporpous outlets of MMSN–NH_2 nanoparticles to prevent the cargo from leaking. DOX/MMSN-NH_2/DNA_{20} complexes were constructed through the amidation reaction between amino groups on the surface of MMSN-NH_2 nanoparticles and carboxyl-functionalized DNA_{20}. Compared with our previous study [38], this method presents the advantage of its simplicity and reliability. The appearance of the peak at 260 nm for DOX/MMSN-NH_2/DNA_{20} complexes was attributed to the DNA absorbance (Fig. 6), indicating the successful capped with DNA_{20}. Zeta potential value of the DOX/MMSN-NH_2/DNA_{20} complexes reversed from 12.7 mV to -5.5 mV due to the conjugation of negative charged DNA_{20} on DOX/MMSNs-NH_2 complexes. On the other hand, the $\nu_{C=O}$ peak appeared at 1686 cm^{-1} in the FTIR spectrum of the DOX/MMSN-NH_2/DNA_{20} complexes, also suggests the successful conjugation of the DNA_{20} on DOX/MMSN-NH_2 complexes.

The controlled release behavior of DOX/MMSN-NH_2/DNA_{20} complexes was performed in PBS buffer with pH 5.0. The pH 5.0 was determined according to previous studies [38-39], which reported that DOX rarely released from nanocarriers in solution with pH 7.4, but the drug release was triggered when the pH value decreased to 5.0. On the other hand, it has demonstrated that the pH environment of cancer cells was nearly pH 7.4, while that of the endosome/lysosome and cytosol in cells was estimated to be pH 5.0–5.5. As shown in Fig.7A, at the temperature of 37°C, less than 10% DOX was released from DOX/MMSN-NH_2/DNA_{20} complexes. However, when the temperature increased to 43°C, more than 50% of DOX was

released, and the DOX release behavior was similar when the temperature further increased to 47 °C. It indicated that the DNA_{20} could cap the mesoporous outlets, and the electrostatic force between DOX/MMSN-NH_2 nanoparticles and DNA_{20} could be destroyed when the temperature increased to 43 °C and 47 ^{o}C. Importantly, the desirable temperature for hyperthermia therapy is range from 43 °C to 47 ^{o}C. In order to evaluate the potential smart release behavior of the nanosystem, a high-low temperature reversal cycle was performed to form "on-off" state. As shown in Fig. 7B, the releasing profile showed that the release of DOX was very slow when the temperature decreased to 37 °C, but the drug release rate speeded up once the temperature increased to 43 ^{o}C. The result indicated that DNA_{20} could successfully cap the mesoporous outlets and control the DOX release behavior. That is to say, a reversible "on-off" mechanism could be realized through DNA_{20}-capped nanosystem. It might be that the amide bond formed between the amino group and carboxyl group was relatively stable under the changed temperature range, which made one terminal of DNA_{20} always to conjugate onto the surface of MMSN-NH_2 nanoparticles. However, the electrostatic interaction between MMSN-NH_2 nanoparticles and another terminal of DNA_{20} would be weaker when the temperature increase, resulting into the detachment of another terminal of DNA_{20} and the opening of the mesoporous outlets. While the temperature decrease to 37 °C, the increase of electrostatic interaction between positive charged MMSN-NH_2 nanoparticles and negative charged DNA_{20} induced the capping of mesoporous outlets again.

3.3. Magnetic heating capacity of MMSN–NH_2 nanoparticles

The presence of magnetic Fe_3O_4 nanoparticles in mesoporous silica matrix ensures the potential of the MMSN–NH_2 nanoparticles to reach hyperthermia temperature range under an alternating magnetic field. The magnetization curve of the MMSN-NH_2 nanoparticles shows a very small hysteresis loop with the coercivity of 3.5 Oe and the remanece of 0.2 emu/g, suggesting the superparamagnetic behavior of MMSN-NH_2 nanoparticles (Fig. 8A). The saturation magnetization value is estimated to be 6.8 emu/g. Therefore, MMSN-NH_2 nanoparticles have potential to generate heat under alternating magnetic field due to their superparamagnetic behavior. Fig. 8B shows the magnetic heating capacity of MMSN–NH_2 nanoparticles evaluated under the magnetic field with a frequency of 409 kHz and magnetic field strength of 180 Gauss. The temperature of the MMSN–NH_2 solutions can increase under an alternating magnetic field, and the magnetic heating capacity enhanced with increasing the concentration of the MMSN–NH_2 solutions. At a concentration of 10 mg/ml, the temperature can be increased to 43 ^{o}C within 539 s, but the time decreased sharply to 45 s when the concentration increased to 50 mg/ml. The results indicated the potential of the MMSN–NH_2 nanoparticles for magnetic hyperthermia.

3.4. In vitro cytotoxicity and cell uptake of the magnetic nanosystems

Investigation of the safety of nanocarriers is significantly important for clinical application. In this study, in vitro cytotoxicities of the MMSN-NH_2, DOX/MMSN-NH_2, and DOX/MMSN-NH_2/DNA_{20} complexes to HeLa cells were evaluated using a Cell

Counting Kit-8 (CCK-8) assay. As shown in Fig. 9(A), after incubation of cells with the MMSN-NH_2, DOX/MMSN-NH_2, and DOX/MMSN-NH_2/DNA_{20} complexes for 24h, negligible cytotoxicity was observed for the MMSN-NH_2 nanoparticles even at a concentration of 100 μg/ml, which suggest that the MMSN-NH_2 nanoparticles used in the study are safe. After loading DOX into the MMSN-NH_2 nanoparticles, the DOX/MMSN-NH_2 complexes showed a significant cytotoxicity to HeLa cells. However, the DOX/MMSN-NH_2/DNA_{20} complexes only showed lower cytotoxicity, suggesting that by capping the mesopores with DNA_{20} could decrease the side-effect during DOX delivery before arriving the targeted cells or organs.

On the other hand, the synergistic effect of chemotherapy and hyperthermia for the magnetic nanosystem was investigated. As shown in Fig 9(B), after treating the complexes with two high-low temperature cycles, the MMSN-NH_2 nanoparticles show a slight cytotoxicity to HeLa cells. It might be that the relative short heating treatment period could not induce a significant hyperthermia effect. Compare with the DOX/MMSN-NH_2 complexes, the DOX/MMSN-NH_2/DNA_{20} complexes showed a lower cytotoxicity because the DOX was blocked in the channels by DNA_{20} capping at 37 ^{o}C. It suggested that the potential therapeutic effect could be realized by introduce DNA_{20} as gatekeeper, and the critical temperature could control the release of DOX.

It is desirable for drug carriers to be taken up by cancer cells, the accurate uptake of drug carriers could enhance of the intracellular delivery efficiency of drugs. On the other hand, the uptake of DOX/MMSN–NH_2 nanoparticles by cancer cells could

facilitate local magnetic hyperthermia owning to magnetic heating in cancer cells. To verify the cell uptake of the DOX/MMSN–NH_2 nanoparticles, the DOX/MMSN–NH_2 nanoparticles were incubated with HeLa cells for 6 h. As shown in Fig. 10, the red fluorescence of DOX facilitates the observation of cell uptake of DOX/MMSN–NH_2 nanoparticles, the fluorescence from DOX/MMSN–NH_2 nanoparticles distributed primarily located between the cell membrane and the nucleus, which probability due to the DOX was release from the nanoparticles after endocytosis. Some previously studies indicated that anticancer drug would release from the carriers after endocytosis, which is similar to CLSM image shown in Fig.10 (B). [40-41].

In order to further identify DOX release from the MMSN nanocarriers after endocytosis, MMSN nanoparticles were labeled with FITC and then loaded DOX in nanocarriers to incubate with HeLa cells for 6 h. Fig. 11 shows CLSM images of HeLa cells after 6 h of incubation with the DOX/MMSN-NH_2-FITC nanoparticles. The green fluorescence from the FITC-labeled MMSN (MMSN–NH_2–FITC) nanoparticles can be clearly observed in HeLa cells, and most of green fluorescence located near cell membranes. Red fluorescence from DOX was distributed in cytoplasm, similar to the results in Fig. 10. It suggested that MMSN-NH_2 nanocarriers could be internalized into HeLa cells and release DOX after endocytosis. Therefore, it can be imagined that loading of anticancer drugs in the MMSN–NH_2 nanoparticles to deliver in cancer cells could significantly enhance the efficiency of drug delivery and magnetic hyperthermia, and thereby promote cancer therapy.

4. Conclusions

In this study, magnetic nanoparticles based smart therapeutic platform for potential smart controllable release of anticancer drug and magnetic hyperthermia has been developed. The results indicated that DOX was loaded in MMSN-NH_2 nanoparticles and could be blocked by carboxyl modified DNA_{20} through amide bond formed between MMSN-NH_2 and DNA_{20} cappers. DOX release could be controlled in reversible manner through temperature change. An in vitro study showed effective cell uptake of MMSN-NH_2 nanoparticles in HeLa cells, and negligible cytotoxicity of MMSN-NH_2 nanoparticles has been observed. Furthermore, MMSN–NH_2 nanoparticles could efficiently generate heat upon exposure to an alternating magnetic field. Therefore, DOX/MMSNs-NH_2/DNA_{20} nanosystem could be a promising therapeutic platform for potential cancer therapy with chemotherapy and magnetic hyperthermia.

Acknowledgements

The authors gratefully acknowledge the support by the Program for Professor of Special Appointment (Eastern Scholar) at Shanghai Institutions of Higher Learning, National Natural Science Foundation of China (No. 51572172), Program for New Century Excellent Talent in University (No. NCET-12-1053), Shanghai Shuguang Project (No. 12SG39) and the Hujiang Foundation of China (No. B14006).

References

1 O.M. Abo-Salem, *J. Biochem. Mol. Toxic.*, 2012, **26**,1-9.

2 Y. Cheng, L. Zhao, Y. Li and T. Xu, *Chem. Soc. Rev.,* 2011, **40**, 2673-2703.

3 M. A. C. Stuart, W. T. S. Huck, J. Genzer, M. Müller, C. Ober, M. Stamm, G. B. Sukhorukov, I. Szleifer, V. V. Tsukruk, M. Urban, F. Winnik, S. Zauscher, I. Luzinov and S. Minko, *Nat. Mater.,* 2010, **9**, 101-113.

4 J. L. Vivero-Escoto, I. I. Slowing, B. G. Trewyn and V. S.-Y. Lin, *Small,* 2010, **6**, 1952-1967.

5 J. Xie, G. Liu, H. S. Eden, H. Ai and X. Chen, *Acc. Chem. Res.,* 2011, **44**, 883-892.

6 J. Gao, H. Gu and B. Xu, *Acc. Chem. Res.,* 2009, **42**, 1097-1107.

7 C. W. Kessinger, O. Togao, C. Khemtong, G. Huang, M. Takahashi and J. Gao, *Theranostics*, 2011, **1**, 263-273.

8 C. D. Kowal and J. R. Bertino, *Cancer Res.*, 1979, **39**, 2285-2289.

9 K.-J. Chen, E.-Y. Chaung, S.-P. Wey, K.-J. Lin, F. Cheng, C.-C. Lin, H. Liu, H.-W. Tseng, C.-P. Liu, M. Wei, C. Liu and H.-W. Sung, *ACS NANO*, 2014, **8**, 5105-5115.

10 H. Kakwere, M. P. Leal, M.-E. Materia, A. Curcio, P. Guardia, D. Niculaes, R. Marotta, A. Falqui and T. Pellegrino, *ACS Appl. Mater. Interfaces,* 2015, **7**, 10132-10145.

11 Y. Wang, B. Li, L. Zhang, H. Song and L. Zhang, *ACS Appl. Mater. Interfaces*, 2013, **5**, 11−15.

12 H. Yu, Z. Cui, P. Yu, C. Guo, B. Feng, T. Jiang, S. Wang, Q. Yin, D. Zhong, X. Yang, Z. Zhang and Y. Li, *Adv. Funct. Mater.*, 2015, **25**, 2489-2500.

13 N. Li, Z. Yu, W. Pan, Y. Han, T. Zhang and B. Tang, *Adv. Funct. Mater.*, 2013, **23**, 2255-2262.

14 C. Park, K. Oh, S.C. Lee and C. Kim, *Angew. Chem. Int. Ed.*, 2007, **46**, 1455-1457.

15 E. Secret, S. J. Kelly, K. E. Crannell and J. S. Andrew, *ACS Appl. Mater. Interfaces*, 2014, **6**, 10313-10321.

16 K. Patel, S. Angelos, W. R. Dichtel, A. Coskun, Y. Yang, J. I. Zink and J. F. Stoddart, *J. Am. Chem. Soc.* 2008, **130**, 2382–2383.

17 B. K. C. Remant, V. Chandrashekaran, B. Cheng, H. Chen, M. M. O. Peña, J. Zhang, J. Montgomery and P. Xu, *Mol. pharmaceutics*, 2014, **11**, 1897-1905.

18 Q. Fu, G. V. R. Rao, L. K. Ista, Y. Wu, B. P. Andrzejewski, L. A. Sklar, T. L. Ward and G. P. Lopez, *Adv. Mater.* 2003, **15**, 1262–1266.

19 Y. Wang, B. Li, L. Zhang, H. Song and L. Zhang, *ACS Appl. Mater. Interfaces*, 2013, **5**, 11-15.

20 J. Liu, C. Detrembleur, M.-C. D. Pauw-Gillet, S. Mornet, L. V. Elst, S. Laurent, C. Jérôme and E. Duguet, *J. Mater. Chem. B*, 2014, **2**, 59-70.

21 S. Kumar, Y. L. Dory, M. Lepage and Y. Zhao, *Macromolecules*, 2011, **44**, 7385-7393.

22 X. Wu, Z. Wang, D. Zhu, S. Zong, L. Yang, Y. Zhong and Y. Cui, *ACS Appl. Mater. Interfaces*, 2013, **5**, 10895-10903.

23 R. P. Johnson, Y. I. Jeong, J. V. John, C.-W. Chung, D. H. Kang, M. Selvaraj, H. Suh and I. Kim, *Biomacromolecules*, 2013, **14**, 1434-1443.

24 C. Li, J. Jin, J. Liu, X. Xu and J. Yin, *ACS Appl. Mater. Interfaces*, 2014, **6**, 13956-13967.

25 Y.-Z. You, K. K. Kalebaila, S. L. Brock and D. Oupick´y, *Chem. Mater.*, 2008, **20**,

3354-3359.

26 E. Climent, R. Martinez-Manez, F. Sancenon, M. D. Marcos, J. Soto, A. Maquieira and P. Amoros, *Angew. Chem. Int. Ed.*, 2010, **49**, 7281-7283.

27 A. Schlossbauer, S. Warncke, P. M. E. Gramlich, J. Kecht, A. Manetto, T. Carell and T. Bein, *Angew. Chem. Int. Ed.*, 2010, **49**, 4734-4737.

28 X. Yang, X. Liu, Z. Liu, F. Pu, J. Ren and X. Qu, *Adv. Mater.*, 2012, **24**, 2890-2895.

29 Y. Chang, P. Liao, H. S. Sheu, Y. J. Tseng, F. Cheng and C. S. Yeh, *Adv. Mater.*, 2012, **24**, 3309-3314.

30 C. Chen, J. Geng, F. Pu, X. Yang, J. Ren and X. Qu, *Angew. Chem. Int. Ed.*, 2011, **50**, 882-886.

31 E. Ruiz-Hernandez, A. Baeza and M. Vallet-Reg ı´, *ACS Nano*, 2011, **5**, 1259-1266.

32 P. Zhang, F. Cheng, R. Zhou, J. Cao, J. Li, C. Burda, Q. Min and J.-J. Zhu, *Angew. Chem. Int. Ed.*, 2014, **53**, 2371-2375.

33 R. Jin, G. Wu, Z. Li, C. A. Mirkin and G. C. Schatz, *J. Am. Chem. Soc.*, 2003, **125**, 1643–1654.

34 A. M. Derfus, G. von Maltzahn, T. J. Harris, T. Duza, K. S. Vecchio, E. Ruoslahti and S. N. Bhatia, *Adv. Mater.*, 2007, **19**, 3932-3936.

35 Z. Yu, N. Li, P. Zheng, W. Pan and B. Tang, *Chem. Commun.*, 2014, **50**, 3494-3497.

36 M.S. Yavuz, Y. Cheng, J. Chen, C. M. Cobley, Q. Zhang, M. Rycenga, J. Xie, C. Kim, K. H. Song, A. G. Schwartz, L. V. Wang and Y. Xia, *Nat. Mater.*, 2009, **8**, 935-939.

37 Y. Zhu, J. Shi, W. Shen, X. Dong, J. Feng, M. Ruan and Y. Li, *Angew. Chem. Int. Ed.*, 2005,**44**, 5083-5087.

38 Y. Zhu and C. Tao, *RSC Adv.*, 2015, **5**, 22365-22372.

39 C. Tao and Y. Zhu, *Dalton T.*, 2014, **43**, 15482-15490.

40 Y. Chen, Y. Gao , H. Chen, D. Zeng, Y. Li, Y. Zheng, F. Li, X. Ji, X. Wang, F. Chen, Q. He, L. Zhang and J. Shi, *Adv. Funct. Mater.,* 2012, **22**, 1586–1597.

41 L. Pan, J. Liu, Q. He, L. Wang and J. Shi, *Biomaterials,*2013 ,**34**, 2719-2730.

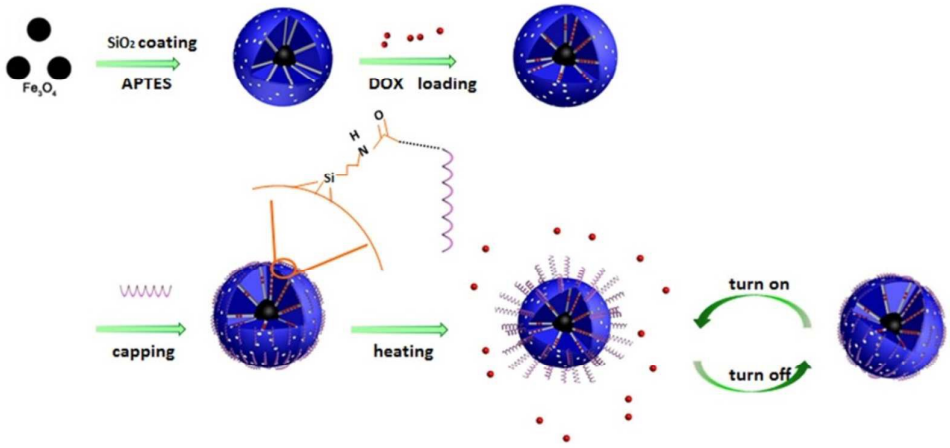

Scheme 1 Schematic of MMSNs based smart therapeutic platform

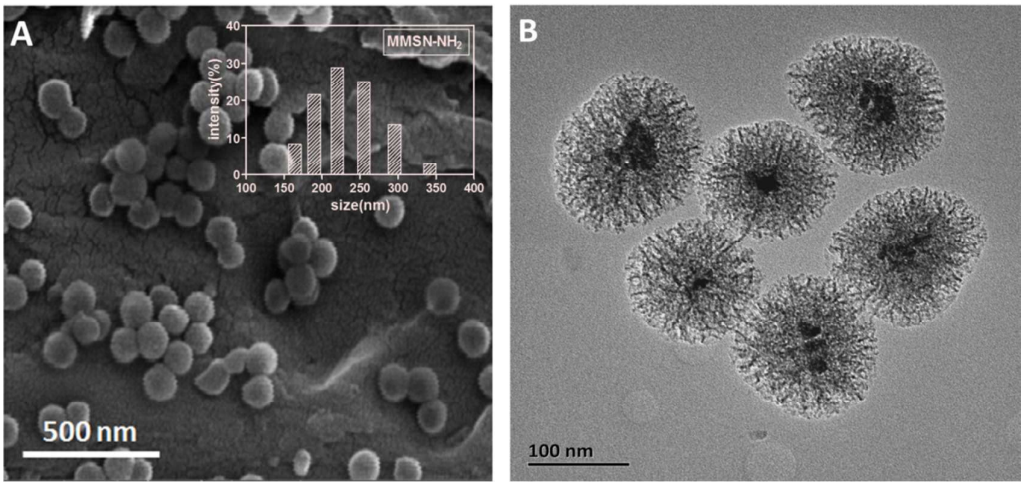

Fig. 1 (A) SEM and (B) TEM images of MMSN-NH_2 nanoparticles.

Inset: size distribution histogram of MMSN-NH_2 nanoparticles

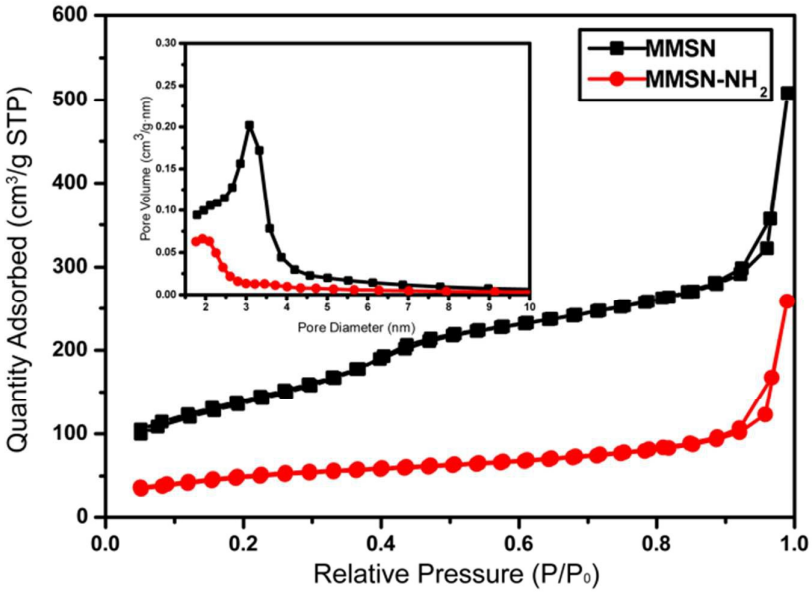

Fig.2 N_2 adsorption-desorption isotherms of the MMSNs and MMSN-NH_2 nanoparticles

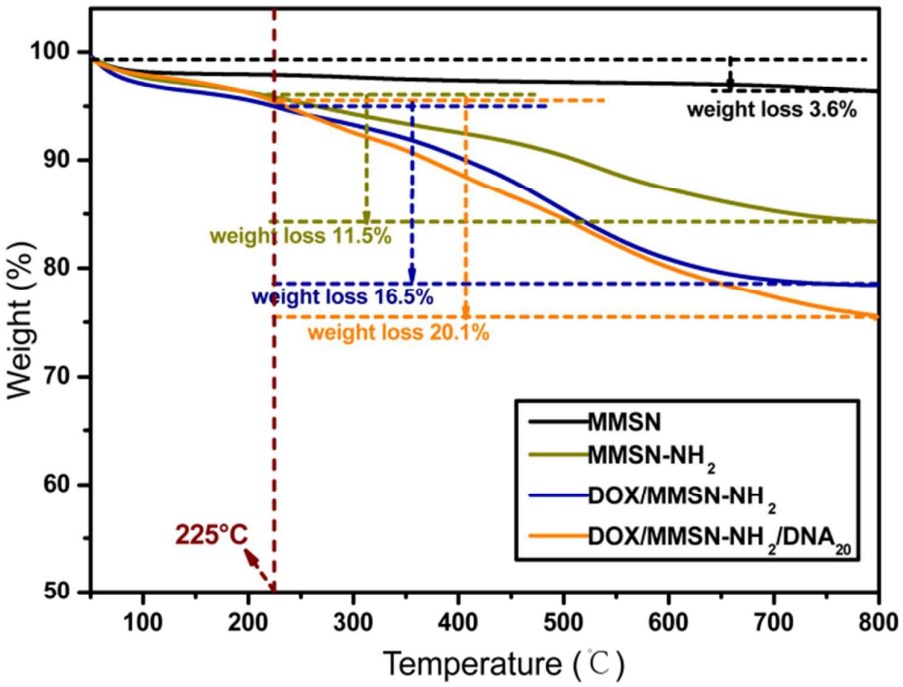

Fig.3 TG analysis of MMSNs, MMSN-NH_2, DOX/MMSN-NH_2 and DOX/MMSN-NH_2/DNA_{20} nanoparticles.

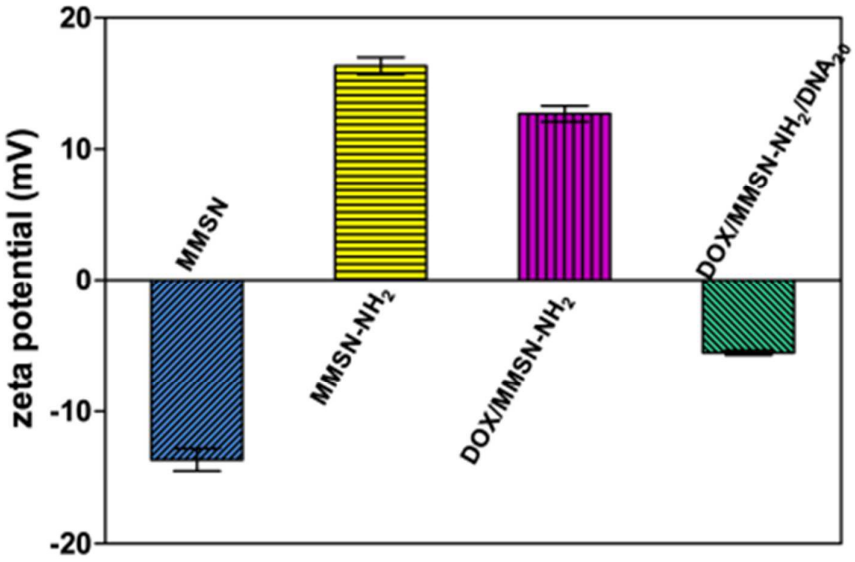

Fig.4 Zeta protential of MMSNs, MMSN-NH_2, DOX/MMSN-NH_2 and DOX/MMSN-NH_2/DNA_{20} nanoparticles.

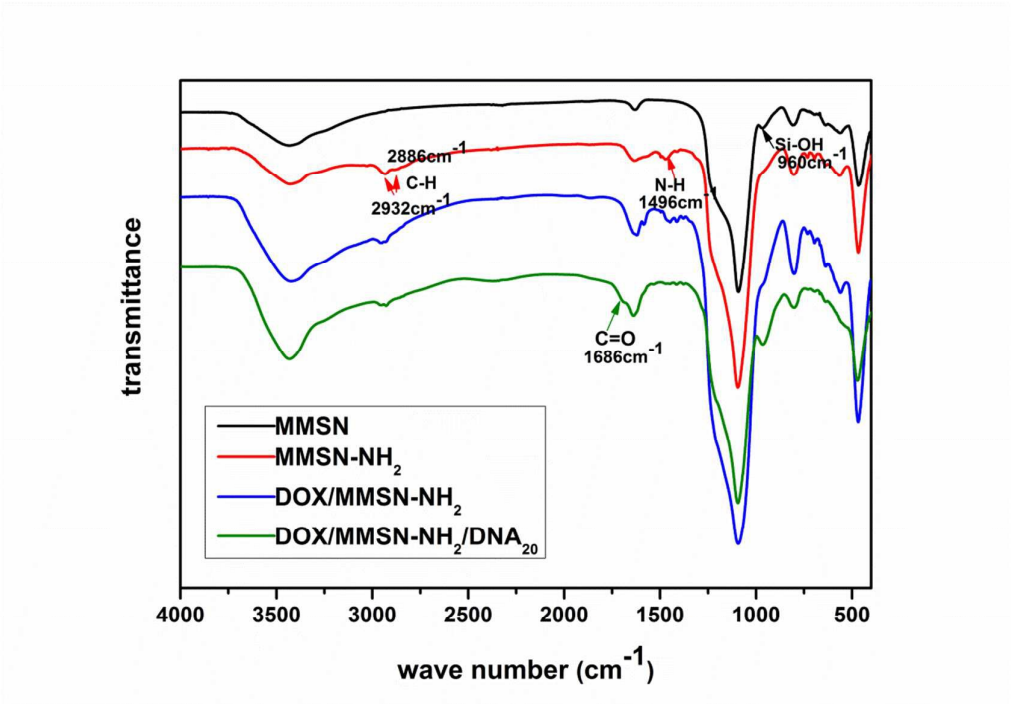

Fig.5 FTIR spectra of MMSNs, MMSN-NH_2, DOX/MMSN-NH_2 and DOX/MMSN-NH_2/DNA_{20} nanoparticles.

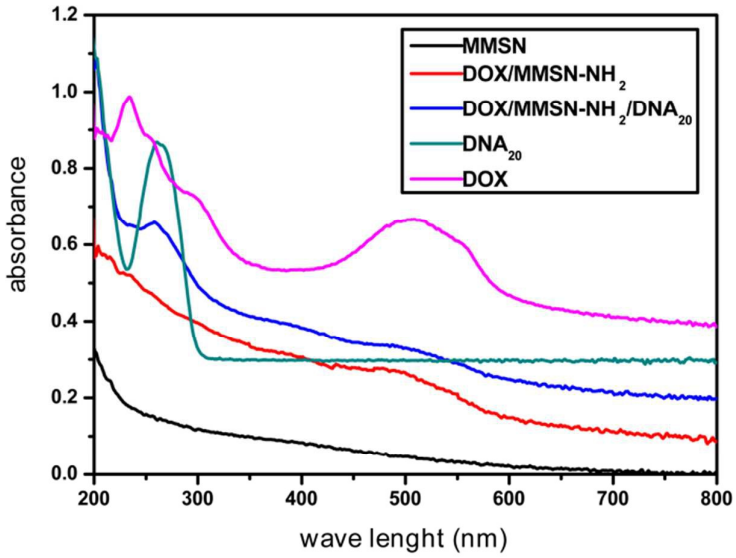

Fig.6 UV-Vis spectra of the MMSNs, DOX/MMSN-NH_2, DOX/MMSN-NH_2/DNA_{20}, DNA_{20} and DOX.

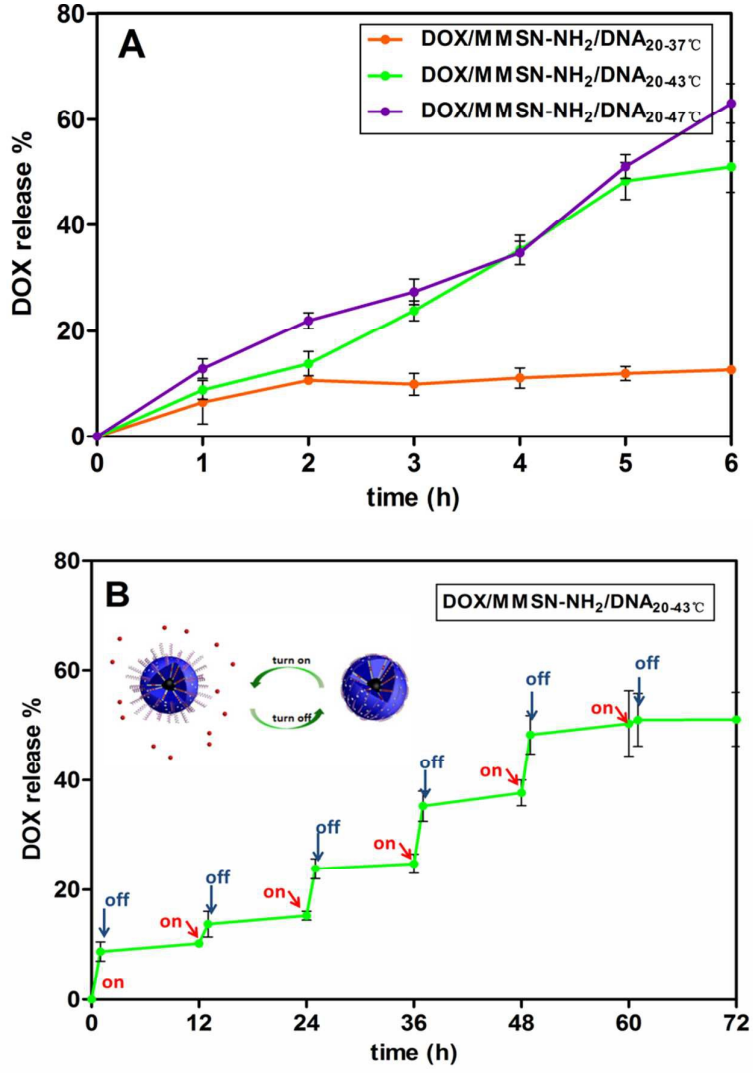

Fig.7 The DOX release profiles of the DOX/MMSN-NH_2/DNA_{20} complexes under different temperature conditions; (B) Controlled release profile of the DOX/MMSN-NH_2/DNA_{20} complexes for 37°C-43°C cycles.

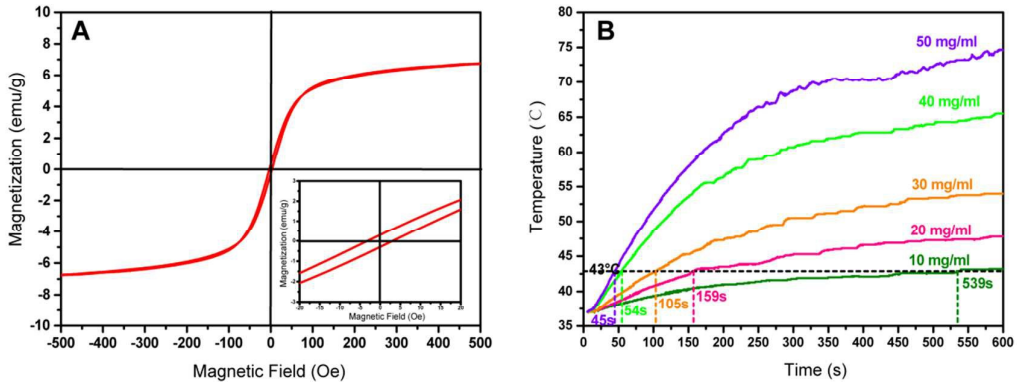

Fig.8 (A) Magnetization curves of MMSN-NH_2 nanoparticles measured at 298 K (B) The magnetic heating capacity of MMSN–NH_2 nanoparticles evaluated under the magnetic field with a frequency of 409 kHz and magnetic field strength of 180 Gauss

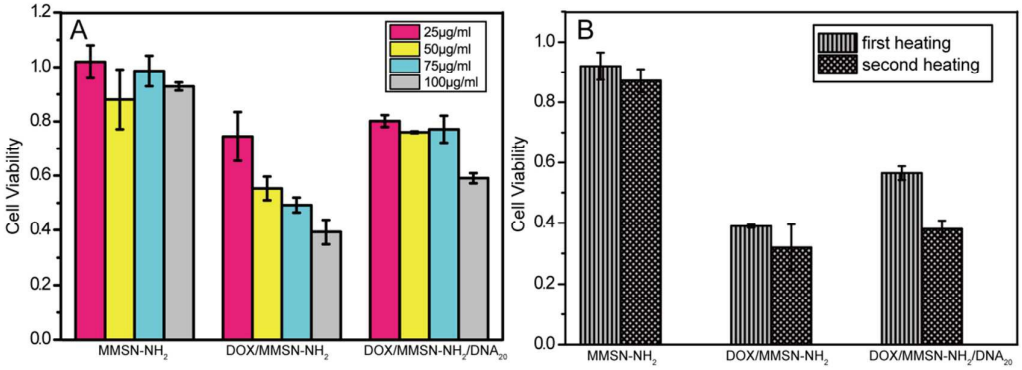

Fig.9 Effect of concentrations of MMSN-NH_2 nanoparticles on the cytotoxicity to HeLa cells, as measured by a Cell Counting Kit-8 assay.

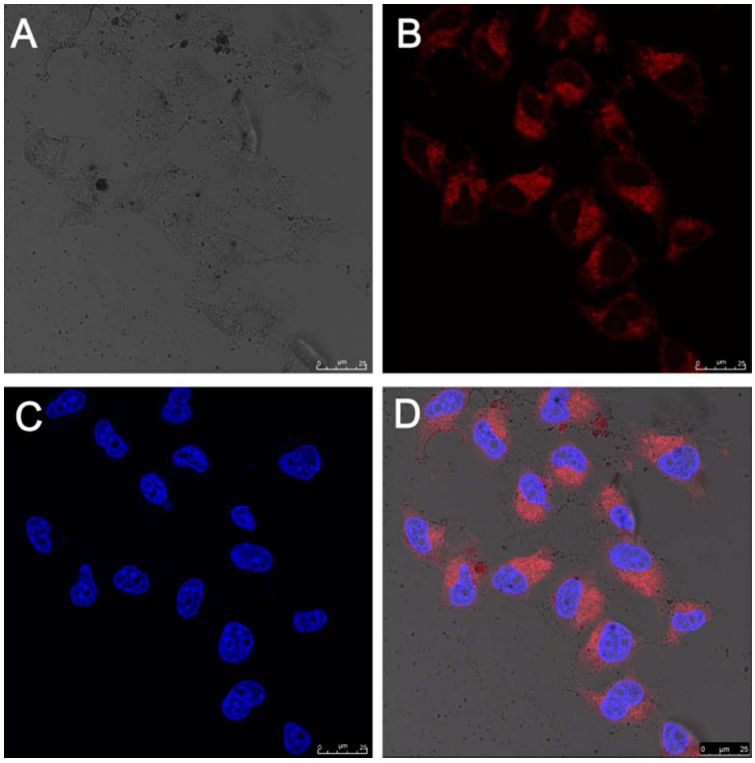

Fig.10 Confocal laser scanning microscope (CLSM) images of HeLa cells after 6h of incubation with the DOX/MMSN-NH_2 nanoparticles: (A) bright field; (B) DOX channel; (C) DAPI channel and (D) merged from bright, DOX and DAPI channels.

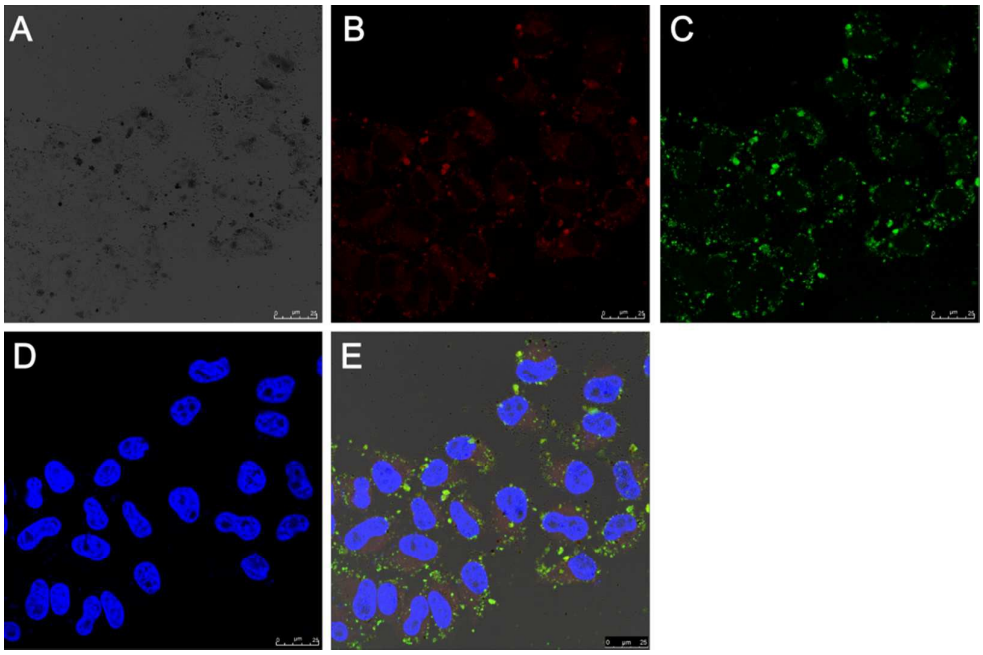

Fig.11 Confocal laser scanning microscope (CLSM) images of HeLa cells after 6h of incubation with the DOX/MMSN-NH_2-FITC nanoparticles: (A) bright field; (B) DOX channel; (C) FITC channel; (D) DAPI channel and (E) merged from bright, DOX, FITC and DAPI channels.

A Table of Contents Entry

Title: Smart Magnetic Nanosystem with Controllable Drug Release and Hyperthermia for Potential Cancer Therapy

Authors: Yi Xu, Yufang Zhu, Stefan Kaskel

TOC Figure:

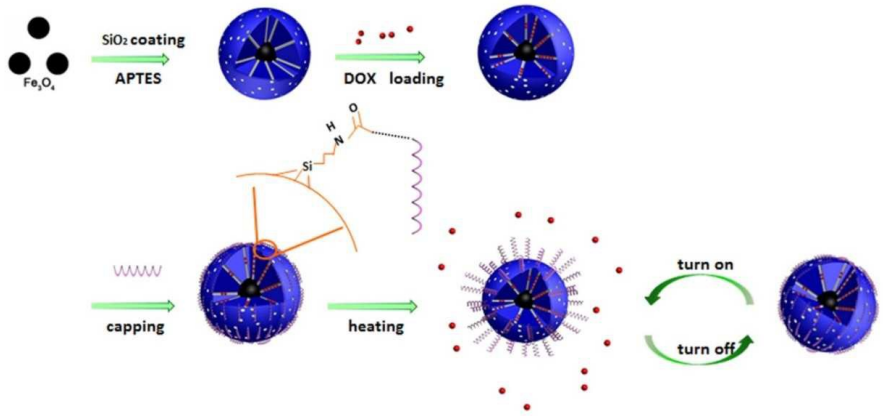

Text: A smart therapeutic platform with potential controllable drug release and magnetic hyperthermia was constructed through the conjugation of carboxyl-modified DNA onto the aminated magnetic mesoporous silica nanoparticles.